DOI: 10.1002/adma.200601882

Spontaneous Formation of Mesoscale Polymer Patterns in an Evaporating Bound Solution**

By *Suck Won Hong*, *Jianfeng Xia*, and *Zhiqun Lin**

The use of spontaneous self-assembly as a lithography- and external-fields-free means to construct well-ordered, often intriguing structures, has received much attention owing to the ease of producing complex structures with small feature sizes.[1–3] Drying mediated self-assembly of nonvolatile solutes (polymers, nanoparticles, and colloids) through irreversible solvent evaporation of a sessile droplet on a solid substrate (unbound solution) represents one such case.[3–16] However, irregular polygonal network structures (Benard cells)[14,15] and stochastically distributed concentric 'coffee rings'[4–6,10] are often observed. The irregular multirings ('coffee rings') are formed via repeated pinning and depinning events (i.e., 'stick-slip' motion) of the contact line.[4–6,10] The evaporation flux varies spatially, with the highest flux observed at the edge of the drop. Therefore, to form spatially periodic patterns at the microscopic scale, the flow field in an evaporating liquid must be delicately harnessed. In this regard, recently, a few attempts have been made to guide the droplet evaporation in a confined geometry[17–20] with[17] or without[18–22] the use of external fields. Patterns of remarkably high fidelity and regularity have been produced.[18–22] However, interfacial interactions between nonvolatile solutes and substrates govern the stability of thin films and have not been explored in these studies. The synergy of controlled self-assemblies of solutes, and their destabilization mediated by the interaction between solutes and substrates during the solvent evaporation, can lead to the formation of intriguing, ordered structures.

Herein, we report on the spontaneous formation of well-organized mesoscale polymer patterns during the course of solvent evaporation by constraining polymer solutions in a sphere-on-Si geometry, as illustrated in Figure 1 (bound solution, i.e., capillary bridge). Gradient concentric rings and self-organized punch–holelike structures were obtained via mediating interfacial interactions between the polymer and the substrate. This facile approach opens up a new avenue for producing yet more complex patterns in a simple, controllable, and cost-effective manner.

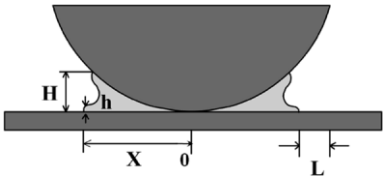

Figure 1. Confined geometry: cross-sectional view of a capillary-held solution containing nonvolatile solutes placed in a sphere-on-Si geometry (i.e., capillary bridge). *X* is the radial distance of a formed pattern away from the center of sphere/Si contact, *h* is the thickness of the thin film, *H* is the height of the capillary bridge at the liquid/vapor interface, and *L* is the distance from the capillary entrance to the meniscus (the liquid/vapor interface).

Poly(methyl methacrylate) (PMMA), polystyrene (PS), and PS-*b*-PMMA diblock copolymers were used as nonvolatile solutes to prepare PMMA, PS, and PS-*b*-PMMA toluene solutions, respectively. The concentration of all the solutions was 0.25 mg mL^{-1}. The evaporation, in general, took less than 30 min to complete. The pattern formation was monitored in situ by using optical microscopy (OM). After the evaporation was complete, two surfaces (spherical lens and Si) were separated and examined by using OM and atomic force microscopy (AFM). Only the patterns on Si were evaluated.

Highly ordered gradient concentric rings of PMMA, persisting toward the sphere/Si contact center, were obtained over the entire surfaces of the sphere and Si except the region where the sphere was in contact with Si (Fig. 2a). A typical OM image of a small region of entire rings of PMMA is shown in Figure 2b. The formation of periodic, gradient rings was a direct consequence of controlled, repetitive 'stick-slip' motion of the contact line, resulting from the competition of linear pinning force and nonlinear depinning force (i.e., capillary force) in the sphere-on-Si geometry[20]. This is in sharp contrast with irregular concentric rings formed in an unbound liquid by stochastic 'stick-slip' motion of the contact line,[5,6,10] suggesting that the use of the sphere-on-Si geometry rendered control over the evaporation rate, and is effective in improving the stability against the convection.

Representative 3D AFM height images of PMMA rings at different radial distances, *X* (Fig. 1), away from the center of the sphere/Si contact are shown in Figure 2c–e. The recession (Fig. 2c–e) of the center-to-center distance between adjacent rings, λ_{C-C}, and the height of the ring, *h*, was clearly evident. As the solution front moved toward the center of the sphere/Si contact due to evaporative loss of toluene (Fig. 2a), both λ_{C-C} and *h* decreased progressively from $\lambda_{C-C} = 35.2$ μm and

[*] Prof. Z. Lin, S. W. Hong, J. Xia
Departments of Materials Science and Engineering, Iowa State University, Ames, IA 50011 (USA)
E-mail: zqlin@iastate.edu

[**] We gratefully acknowledge the supports from the 3M nontenured faculty award and the American Chemical Society Petroleum Research Fund (Grant No. 42825-G7). Supporting Information is available online at Wiley InterScience or from the author.

ADVANCED MATERIALS

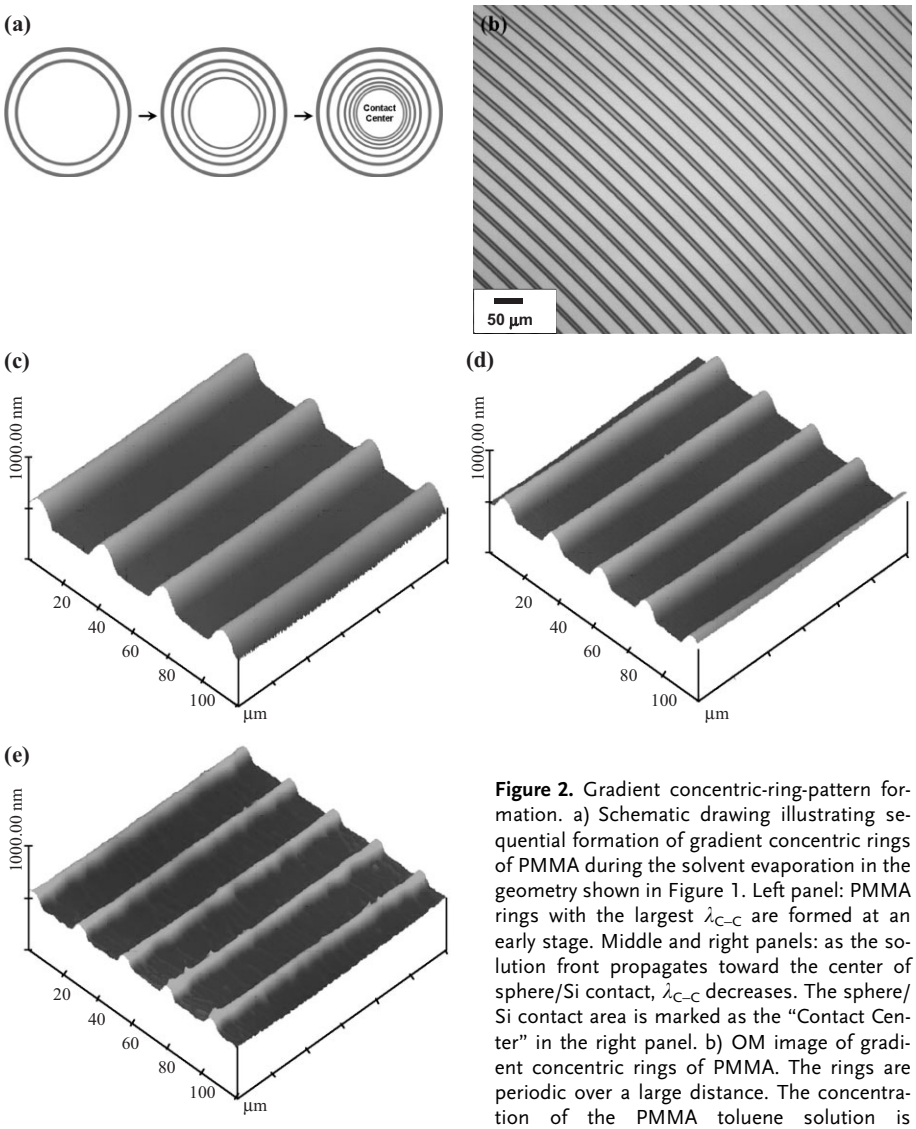

Figure 2. Gradient concentric-ring-pattern formation. a) Schematic drawing illustrating sequential formation of gradient concentric rings of PMMA during the solvent evaporation in the geometry shown in Figure 1. Left panel: PMMA rings with the largest λ_{C-C} are formed at an early stage. Middle and right panels: as the solution front propagates toward the center of sphere/Si contact, λ_{C-C} decreases. The sphere/Si contact area is marked as the "Contact Center" in the right panel. b) OM image of gradient concentric rings of PMMA. The rings are periodic over a large distance. The concentration of the PMMA toluene solution is $c = 0.25$ mg mL^{-1}. The scale bar is 50 μm. c–e) 3D AFM height images of PMMA rings as the 'stick-slip' motion progressively approaches the center of the sphere/Si contact, corresponding to the stages in (a). The image size is 100 μm × 100 μm. The *z* scale is 1000 nm.

$h = 192$ nm at $X = 4200$ μm (Fig. 2c) to 27.2 μm and 141 nm at $X = 3300$ μm (Fig. 2d) to 25.3 μm and 93 nm at $X = 2700$ μm (Fig. 2e). The number of the rings in the 120 μm × 120 μm scan area increased from four rings (Fig. 2c) to four and a half rings (Fig. 2d) to five rings (Fig. 2e). The average width of a typical ring, *w*, was roughly 2–3 orders of magnitude smaller than its associated length (i.e., circumference) (e.g., $(2\pi \times X)/w = 2\pi \times 4200/16.8 \sim 10^3$; corresponding to the rings shown in Fig. 2c). It is noteworthy that marginal undulations at edges of the rings were seen at the very late stage of dynamic self-assembly of PMMA (Fig. 2e), in which the solution front was close to the center of the sphere/Si contact. Such gradient concentric PMMA rings may be explored as unique surfaces for studying cell adhesion, selective adsorption, and molecular recognition.[19]

Rather than a periodic family of concentric rings of PMMA formed by the 'stick-slip' motion of the contact line, considerable fingering instabilities[2,3,7,13,17,23] were observed in the deposition of PS as toluene evaporated, characterized by the appearance of surface perturbation with a well-defined wavelength at edges of a ring (Fig. 3). In the experiment, the concentric rings of PS were found to form only at distances far away from the center of the sphere/Si contact (i.e., at larger *X*) at the early stage of the dynamic self-assembly process (left panel in Fig. 3a), as shown in a representative AFM image (leftmost ring in Fig. 3c). As the solution front progressed inward, fingering instabilities emerged at both sides of a ring (middle panel in Fig. 3a; rightmost ring in Fig. 3c and d) due to the simultaneous occurrence of the 'stick-slip' motion of the contact line and the fingering instabilities of the rings.[17] The fingers were readily revealed in the 2D AFM height images (Fig. 3c and d). Eventually, the contact line jumped inward to a new position, during which it dragged fingers formed in its front with it and yielded the punch–holelike structures, residing along the space between two adjacent rings (see snapshots in Fig. S1 in the Supporting Information, from a real-time lapse video). An OM image is shown in Figure 3b, illustrating surface patterns of PS produced locally at different stages.

The center-to-center distance between adjacent PS fingers on a ring, λ_F, and the height of the ring, *h*, were 26.6 μm and 374 nm, respectively, at $X = 3195$ μm (Fig. 3d) and 25.3 μm and 328 nm, respectively, at $X = 3020$ μm (Fig. 3e, where λ_F was roughly equal to the diameter of the microscopic hole). The average width of fingers at the center connecting two adjacent rings was ca. 2.6 μm, as measured by using AFM (Fig. 3e). The spatial-temporal evolution of PS surface patterns from rings to fingers to microscopic holes can be rationalized as follows. The velocity of the displacement of the meniscus (i.e., the liquid/vapor interface), *v*, in a capillary bridge is inversely proportional to the distance from the capillary entrance to the meniscus, *L* (Fig. 1) (i.e., $v \sim 1L$).[24] *v* deceases as the meniscus moves inward as a result of an increase in *L*. Numerical calculations have demonstrated that the formation

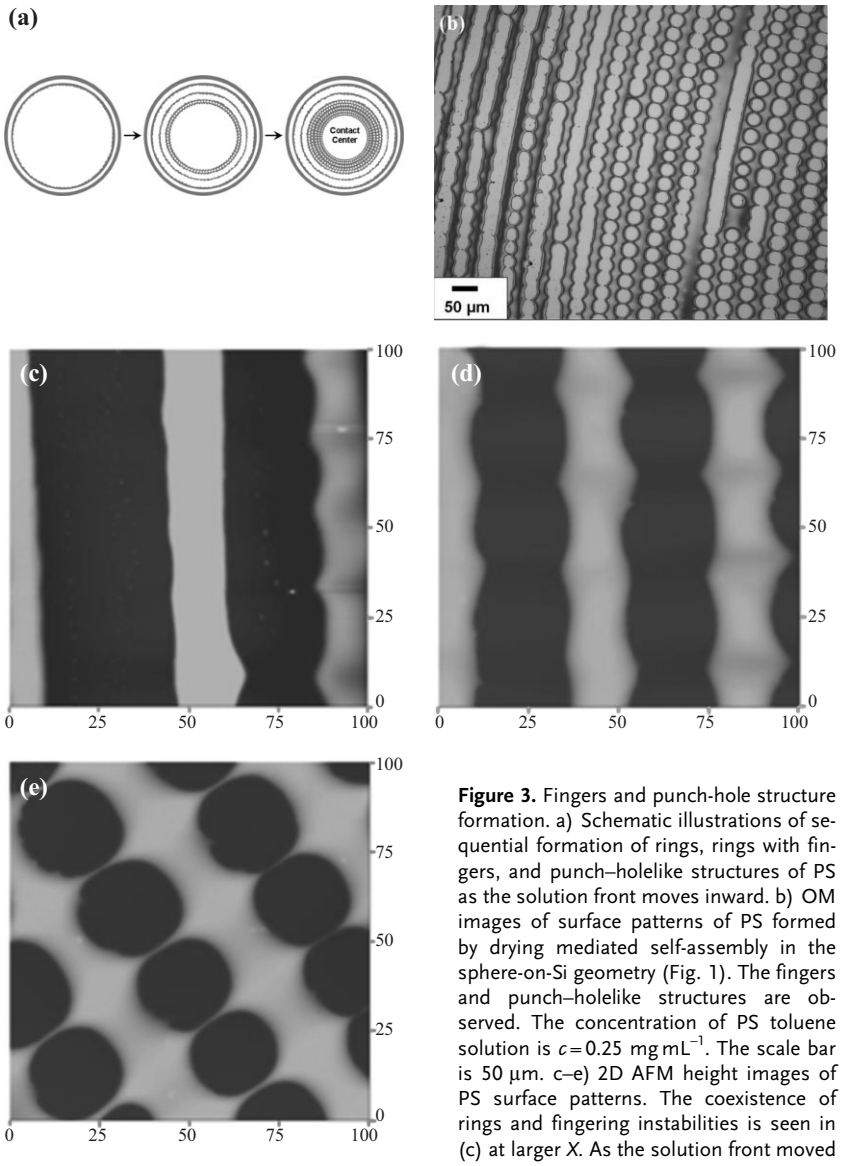

Figure 3. Fingers and punch-hole structure formation. a) Schematic illustrations of sequential formation of rings, rings with fingers, and punch–holelike structures of PS as the solution front moves inward. b) OM images of surface patterns of PS formed by drying mediated self-assembly in the sphere-on-Si geometry (Fig. 1). The fingers and punch–holelike structures are observed. The concentration of PS toluene solution is $c = 0.25$ mg mL^{-1}. The scale bar is 50 μm. c–e) 2D AFM height images of PS surface patterns. The coexistence of rings and fingering instabilities is seen in (c) at larger X. As the solution front moved inward (i.e., reducing X) owing to the evaporative loss of the solvent, fingering instabilities appear at both sides of a ring in (d) and (e). With increasing proximity to the center of the sphere/Si contact, punch–holelike structures are formed in (e). The image size is 100 μm × 100 μm. The z scale is 1000 nm.

of fingering instability in an evaporating film is dictated by v: a faster v stabilizes the front, whereas a slower v leads to the development of fingering instabilities at a propagating front.[25] In the present study, the concentration of the solution was higher at the beginning of the evaporation process so that more solutes can deposit to form a ring, yielding a larger value of h, as observed experimentally. As the solution front retracted, the evaporation rate of the solvent decreased, which, in turn, caused a reduction in v. Thus, fewer solutes were available with which to pin the contact line. As a consequence, the concentration and the viscosity of the solution at the capillary edge decreased. These led to instabilities.[25] The fingers on the PS rings were observed to emerge gradually (middle panel in Fig. 3a, and Fig. 3d). A slower v made fingers more stable. Furthermore, the center-to-center distance between two adjacent rings, λ_{C-C} decreased as rings neared to the center of the sphere/Si contact. This facilitated the continuity of fingers connecting between neighboring rings. The microscopic holes were, thus, formed with increasing proximity to the center of the sphere/Si contact (right panel in Fig. 3a, and Fig. 3e).

Since the solution concentration ($c = 0.25$ mg mL^{-1}), the loading volume ($V = 20$ μL), and the solvent (toluene) were kept the same for both PS and PMMA solutions, the difference in resulting surface patterns of PS and PMMA (i.e., rings in PMMA vs. rings together with fingers and holes in PS) can be attributed to different interfacial interaction between the polymer and the substrate. The in situ OM observation revealed that the formation of fingers at the early stage was a thin-film instability in origin (see snapshots in Fig. S1 in the Supporting Information from the real-time lapse video). On the basis of linear stability analysis on a liquidlike thin film, that is, the capillary edge with height h (Fig. 1) in the present study, the dispersion relation that quantifies the perturbation is given by[26,27]

$$\Omega = -q^4 + \frac{A}{2\pi h^4 \gamma} q^2 \quad (1)$$

where Ω is the growth rate of the perturbation, q is the growth mode, γ is the surface tension of the solute, and A is the Hamaker constant, signifying the interfacial interaction between the solute and the substrate. It has been shown both experimentally and theoretically that a PMMA thin film is stable on a Si surface with 2 nm thick native silicon oxide at the surface, since A is negative.[28,29] In contrast, a PS thin film is unstable owing to a positive value of A.[29–31] Therefore, PMMA rings were stable on a Si substrate, whereas PS rings destabilized and formed fingering instabilities with a fast growth mode,

$$q_m = [1/(2\ h^2)] \times [A/\pi\gamma]^{1/2} \quad (2)$$

It is worth noting that the viscosities of PS and PMMA, which contributed the pinning of the polymers, were of the same order of magnitude provided that number-average molecular weight (M_n) of PS = 420 kg mol^{-1} and PMMA = 534 kg mol^{-1}; however, the stabilities of the polymer rings were governed by the sign of A (Eq. 1). The fingering instabilities were caused by the concentration-gradient-induced surface-tension gradient.[17] The deposition of polymer to form a ring reduced local

ADVANCED MATERIALS

surface tension of the solution, thereby leading the solution to spread to the region with higher concentration.[17] The condition for equilibrium between a wetting and a meniscus is the equality of the capillary pressure and the disjoining pressure,[24]

$$\frac{2\gamma_{\text{meniscus}}}{H} \cong \frac{|A|}{6\pi h^3} \tag{3}$$

Substituting Equation 3 into Equation 2, the characteristic wavelength of fingering instabilities, λ_F is, thus, given by[24,26,27,32]

$$\lambda_F = \frac{2\pi}{q_{\text{m}}} = 2\pi\left(\frac{6\gamma_{\text{meniscus}}}{\gamma hH}\right)^{-\frac{1}{2}} \tag{4}$$

where γ_{meniscus} is the surface tension of the meniscus in the capillary bridge (i.e., the surface tension of toluene in the present study, 29 mN/m), γ is the surface tension of the solute (i.e., the surface tension of PS in present study, 40.7 mN/m), and H is the height of capillary bridge at the liquid/vapor interface (Fig. 1) and can be calculated based on $H \approx X^2/2R$, where R is the radius of curvature of the spherical lens ($R \sim 2$ cm), and X can be readily determined experimentally. Substituting the height of the PS ring, determined by using AFM measurements, and H into Equation 2 yields $\lambda_F = 29.6$ μm at $X = 3195$ μm and $\lambda_F = 26.3$ μm at $X = 3020$ μm, which are in good agreement with values measured experimentally (i.e., 26.6 μm at $X = 3195$ μm in Fig. 3d and 25.3 μm at $X = 3020$ μm in Fig. 3e). While optimized experimental conditions are required to impart higher regularity of punch–holelike structures (Fig. 3b and e), the present findings suggest that a coupling of 'stick-slip' motion and fingering instabilities due to unfavorable interfacial interaction between the nonvolatile solute and the substrate (i.e., possessing a positive A) may provide a unique means of organizing materials into well-ordered structures in which regular microscopic holes reside along concentric circles (Fig. 3e).

To further verify that unfavorable interfacial interaction between PS and the Si substrate is crucial in forming fingering instabilities, a lamellar-forming diblock copolymer of PS-*b*-PMMA was employed as a nonvolatile solute in which PS blocks were covalently linked with PMMA blocks at one end. Figure 4 shows a surface pattern of PS-*b*-PMMA formed by drying mediated self-assembly of a 0.25 mg mL^{-1} PS-*b*-PMMA toluene solution in the sphere-on-Si geometry (Fig. 1). Well-ordered gradient concentric rings of PS-*b*-PMMA formed at the early stage of the solvent evaporation were seen to transform into concentric rings with fingering instabilities at their front at the final stage. The latter reflected a delicate balance of competition of unfavorable interfacial interaction between the PS block and Si and favorable interfacial interaction between the PMMA block and Si. The observations of PS-*b*-PMMA fingers at the final stage contrast significantly with those in homopolymer PMMA, in which

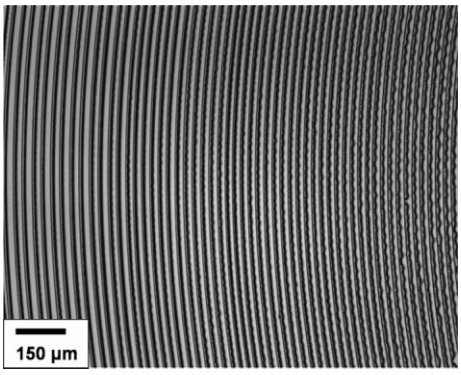

Figure 4. OM image of a gradient concentric surface pattern of a PS-*b*-PMMA diblock copolymer formed from a 0.25 mg mL^{-1} PS-*b*-PMMA toluene solution. As the solution front progresses inward, the transition from rings to the coexistence of rings with fingering instabilities are clearly evident. However, punch-hole-like structures are not observed.

only minimal undulations were detected (Fig. 2). On the other hand, as compared to the case of homopolymer PS (Fig. 3), the punch–holelike structures are, however, not observed in PS-*b*-PMMA. This can be attributed to favorable interaction between the PMMA block and the Si substrate. Depending on the affinity of the respective block for the substrate surfaces and the film thickness, the mircodomain of a block copolymer can be oriented normal to the surface of a film over a large area.[33] A systematic study of microphase separation in the PS-*b*-PMMA rings is currently underway.

In conclusion, we have developed a simple route to produce well-ordered patterns in an easily controllable and cost-effective manner by allowing a drop to evaporate in a sphere-on-Si geometry. The interfacial interaction between the solute and the substrate effectively mediate the pattern formation. The rings and punch-hole-like structures organized in a concentric mode may offer possibilities for many applications, including annular Bragg resonators for advanced optical-communication systems[34] and as tissue-engineering scaffolds.[35,36] The present studies provide valuable insights into the rationale of harnessing the flow and the evaporation process in confined geometries and creating unprecedented regular patterns.

Experimental

Sample Preparation: 0.25 mg mL^{-1} of PS ($M_n = 420$ kg mol^{-1}, the polydispersity, PDI = 1.15), 0.25 mg mL^{-1} of PMMA ($M_n = 534$ kg mol^{-1}, PDI = 1.57), and 0.25 mg mL^{-1} of a lamellar-forming diblock copolymer of PS-*b*-PMMA (M_n of PS = 130 kg mol^{-1}, M_n of PMMA = 133 kg mol^{-1}, PDI = 1.10) toluene solutions were prepared. All solutions were filtered by using a 200 nm filter. The spherical lenses and Si substrates were cleaned by using a mixture of sulfuric acid and Nochromix. Subsequently, they were rinsed with deionized water extensively and blow-dried with N_2.

Confined Geometry: To construct a confined geometry, a spherical lens made from fused silica with a radius of curvature of ca. 2 cm and a Si wafer were used. The sphere and Si were firmly fixed at the top and the bottom, respectively, of the sample holders. To implement a confined geometry, an inchworm motor with a step motion of a few micrometers was used to place the upper sphere into contact with the

lower stationary Si surface. Before they contacted (i.e., separated by approximately a few hundred micrometers apart), a drop of ca. 20 μL polymer toluene solutions were loaded and trapped within the gap between the sphere and Si due to the capillary force. The sphere was finally brought into contact with the Si substrate by using an inchworm motor such that a capillary-held polymer solution (i.e., capillary bridge) formed with the evaporation rate being highest at the extremity (Fig. 1).

Characterization: An Olympus BX51 optical microscope in the reflection mode was used to monitor the patterns formation in real time. AFM images on patterns formed on a Si surface were performed using a Dimension 3100 scanning force microscope in tapping mode (Digital Instruments). BS-tap300 tips (Budget Sensors) with spring constants ranging from 20 to 75N m^{-1} were used as scanning probes.

Received: August 17, 2006
Revised: November 18, 2006
Published online: April 18, 2007

[1] Y. Lin, A. Boker, J. He, K. Sill, H. Xiang, C. Abetz, X. Li, J. Wang, T. Emrick, S. Long, Q. Wang, A. Balazs, T. P. Russell, *Nature* **2005**, *434*, 55.
[2] M. Gleiche, L. F. Chi, H. Fuchs, *Nature* **2000**, *403*, 173.
[3] J. Huang, F. Kim, A. R. Tao, S. Connor, P. D. Yang, *Nat. Mater.* **2005**, *4*, 896.
[4] R. D. Deegan, O. Bakajin, T. F. Dupont, G. Huber, S. R. Nagel, T. A. Witten, *Nature* **1997**, *389*, 827.
[5] R. D. Deegan, *Phys. Rev. E: Stat. Phys., Plasmas, Fluids, Relat. Interdiscip. Top.* **2000**, *61*, 475.
[6] R. D. Deegan, O. Bakajin, T. F. Dupont, G. Huber, S. R. Nagel, T. A. Witten, *Phys. Rev. E: Stat. Phys., Plasmas, Fluids, Relat. Interdiscip. Top.* **2000**, *62*, 756.
[7] O. Karthaus, L. Grasjo, N. Maruyama, M. Shimomura, *Chaos* **1999**, *9*, 308.
[8] E. Rabani, D. R. Reichman, P. L. Geissler, L. E. Brus, *Nature* **2003**, *426*, 271.
[9] Z. Mitov, E. Kumacheva, *Phys. Rev. Lett.* **1998**, *81*, 3427.
[10] E. Adachi, A. S. Dimitrov, K. Nagayama, *Langmuir* **1995**, *11*, 1057.
[11] L. Shmuylovich, A. Q. Shen, H. A. Stone, *Langmuir* **2002**, *18*, 3441.
[12] T. P. Bigoni, X. M. Lin, T. T. Nguyen, E. I. Corwin, T. A. Witten, H. M. Jaeger, *Nat. Mater.* **2006**, *5*, 265.
[13] H. Hu, R. G. Larson, *Langmuir* **2005**, *21*, 3963.
[14] V. X. Nguyen, K. J. Stebe, *Phys. Rev. Lett.* **2002**, *88*, 164 501.
[15] M. Maillard, L. Motte, M. P. Pileni, *Adv. Mater.* **2001**, *13*, 200.
[16] A. J. F. Carvalho, M. A. Pereira-da-Silva, R. M. Faria, *Eur. Phys. J. E* **2006**, *7*, 309.
[17] H. Yabu, M. Shimomura, *Adv. Funct. Mater.* **2005**, *15*, 575.
[18] Z. Q. Lin, S. Granick, *J. Am. Chem. Soc.* **2005**, *127*, 2816.
[19] S. W. Hong, J. Xu, J. Xia, Z. Q. Lin, F. Qiu, Y. L. Yang, *Chem. Mater.* **2005**, *17*, 6223.
[20] J. Xu, J. Xia, S. W. Hong, Z. Q. Lin, F. Qiu, Y. L. Yang, *Phys. Rev. Lett.* **2006**, *96*, 066 104.
[21] S. W. Hong, J. Xu, Z. Q. Lin, *Nano Lett.* **2006**, *6*, 2949.
[22] S. W. Hong, S. Giri, V. S. Y. Lin, Z. Q. Lin, *Chem. Mater.* **2006**, *18*, 5164.
[23] A. M. Cazabat, F. Heslot, S. M. Troian, P. Carles, *Nature* **1990**, *346*, 824.
[24] N. V. Churaev, *Liquid and Vapor Flows in Porous Bodies: Surface Phenomena*, Vol. 13, Gordon and Breach Science University of Salford, UK, **2000**.
[25] A. V. Lyushnin, A. A. Golovin, L. M. Pismen, *Phys. Rev. E: Stat. Nonlinear, Soft Matter Phys.* **2002**, *65*, 021 602.
[26] I. Leizerson, S. G. Lipson, A. V. Lyushnin, *Langmuir* **2004**, *20*, 291.
[27] A. Sharma, *Langmuir* **1993**, *9*, 861.
[28] Z. Q. Lin, T. Kerle, T. P. Russell, E. Schaffer, U. Steiner, *Macromolecules* **2002**, *35*, 6255.
[29] M. D. Morariu, E. Schaffer, U. Steiner, *Eur. Phys. J. E* **2003**, *4*, 375.
[30] G. Reiter, *Phys. Rev. Lett.* **1992**, *68*, 75.
[31] R. Xie, A. Karim, J. F. Douglas, C. C. Han, R. A. Weiss, *Phys. Rev. Lett.* **1998**, *81*, 1251.
[32] W. Zhao, M. H. Rafailovich, J. Sokolov, L. J. Fetters, R. Palno, M. K. Sanyal, S. K. Sinha, B. B. Sauer, *Phys. Rev. Lett.* **1993**, *70*, 1453.
[33] Z. Q. Lin, D. H. Kim, X. D. Wu, L. Boosahda, D. Stone, L. LaRose, T. P. Russell, *Adv. Mater.* **2002**, *14*, 1373.
[34] J. Scheuer, W. M. J. Green, A. Yariv, *Photonics Spectra*, May **2005**.
[35] G. M. Gratson, M. Xu, J. A. Lewis, *Nature* **2004**, *428*, 386.
[36] J. A. Lewis, G. M. Gratson, *Mater. Today* **2004**, *7*, 32.

